Mobile Robot Navigation Amidst Humans with Intents and Uncertainties: A Time Scaled Collision Cone Approach

Akhil Nagariya [1], Bharath Gopalakrishnan [1],Arun Kumar Singh[2], Krishnam Gupta [1] and K.Madhava Krishna[1]

***Abstract*— We propose a novel collision avoidance formulation in the intent space, suitable for navigation of non-holonomic robots in human centered environments. The intent space is characterized by various bands of trajectories wherein each band can be thought to be a representation of a possible human intended motion and the uncertainty associated with it. We ascribe probabilities to human intentions and characterize the uncertainty around it through Gaussian state transition and its concomitant Gaussian parametric distribution. Given an intent space we design avoidance maneuvers based on our recent works on *time scaled collision cone* concept which provides analytical characterization of collision free velocities in dynamic environments. In this paper, we present a probabilistic variant of the *time scaled collision cone* which allows us to relate space of collision free velocities to an associated confidence measure. We also develop an optimization framework which extract such specific solutions from the entire solution space that achieves an elegant balance between the objective of minimizing risk and ease of avoidance maneuver. We further show that by accounting for possible intents in human motion, the method transcends the realm of reactive avoidance to proactive anticipation of collisions and its effective avoidance,thereby increasing the overall safety of navigation.**

I. INTRODUCTION

As robots and humans begin to occupy the same workspaces human centred and human aware navigation are becoming popular [1], [2]. An important theme here is to account for human intents in robot's navigation and avoidance maneuver. For example, while moving in a corridor parallel to the human as shown in figure 1(a) it appears that there are no collisions in discernible future. However the human can swing around the intersection in multiple possible ways surprising the robot with high possibilities of collision as shown in (1(b)). We denote and identify such possibilities of future motion as intents. These typically arise due to a diverse set of potential destinations or waypoints that the robot is unable to foresee or predict purely based on the current trajectory of the human. By anticipating such intents and incorporating them in robots' avoidance behavior we expect to increase the overall safety of the navigation system.

However, such explicit incorporation of intents come at a cost. Firstly, it reduces the solution space of collision free velocities for the robot and second it increases computational load as the robot is now entailed to consider a much larger set of obstacle trajectories for collision avoidance. In this paper, we provide a novel method for collision avoidance incorporating human intents even as we ensure that the robot is not bogged down with a plethora of computations or a rapidly shrinking solution space. The crux of the paper lies in our recently developed concept of *time scaled collision cone* [3] and [4] which allows us to obtain a path constrained version of collision cone constraints.

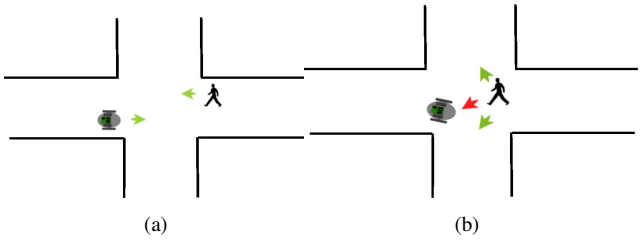

Fig. 1. (a) Shows a typical scenario if the person and robot move along the direction shown by green arrow there is no collision (b) shows that if the person follows the red arrow then there is a possibility of collision

Specifically, the paper contributes in the following ways. Firstly, it introduces a probabilistic variant of *time scaled collision cone* constraints which allows us to relate space of collision free velocities to an associated confidence measure. Secondly, it develops an optimization framework for extracting a specific solution from the entire solution space of collision free velocities.

The third important contribution of the paper is the real time experimental implementation of the proposed collision avoidance framework on a P3DX mobile robot. The experimental implementation itself builds upon a sophisticated yet computationally simple modeling of human intents and trajectories through a Hidden Markov Model (HMM) and Gaussian state transition.

II. RELATED WORK

The problem of collision avoidance is well studied in robotics literature. One of the popular paradigms involves the velocity obstacle introduced in [6] and a similar theme of collision cone in [7]. These were elegantly extended to incorporate multiple holonomic robots [8]. Later, various modifications were proposed to incorporate car like obstacles in the velocity obstacle or collision cone framework [8], [9]. The use of sampling based planners for dynamic obstacle avoidance has also been a well studied problem. For example [10] searches in the combined set of space-time for obtaining collision avoiding trajectories. Whereas, [11] brings in the notion of obstacle uncertainty by modeling it as a Gaussian Process. In more recent times the use of social force model has become popular through the works like [12].

[1] Robotics Research Center, IIIT-Hyderabad India, [2] Bio-Medical Robotics Lab, BGU, Israel arunkima@post.bgu.ac.il, bharath.gopalakrishnan@research.iiit.ac.in, mkrishna@iiit.ac.in

This work builds upon the elegance and effectiveness of non-linear time scaling as an alternate way of solving collision avoidance problem.First introduced in [13] for providing dynamically stable maneuver in uneven terrain ,its efficacy in co-operative reactive collision avoidance with several non holonomic robot trajectories was portrayed in [3]. Centrally it showed that collision avoidance can be modeled as a search in the space of a single variable scale (that is derived in closed form) that appropriately stretches and contracts time (in a non-linear fashion) and thereby robot velocities for collision avoidance. Later, in [4] uncertainty in obstacle states was considered and rapid computation of space of collision free velocities was effectively shown.

The rest of the paper is organized as follows. The paper starts with the description of the proposed intent prediction methodology in section III. We briefly describe the process of characterizing the uncertainty associated with the trajectory towards a particular intent in section IV. Section V reviews the concept of *time scaled collision cone* constraints and then introduces its probabilistic variant. We also explain how it is possible to even obtain a closed form solution of the probabilistic variant of *time scaled collision cone* constraints. Section VI describes the methodology of collision avoidance in the intent space. Specifically, we propose an optimization framework for extracting a particular solution from the entire solution space. Among other factors, this extraction procedure explicitly depends on the intent probabilities. At appropriate places in this section, we substantiate and validate the theoretical exposition with extensive simulation results. The real time implementation of the proposed framework is shown in section VII.

III. Human Intentions Prediction

A. Overview

Human motion prediction is an essential part of an autonomous system that allows a robot to navigate in an indoor environment. Here we propose an HMM based approach to predict human intentions which uses Bayesian human motion intention predictor-BHMIP [14].Reader not familiar with HMMs is referred to [15] for an excellent tutorial.

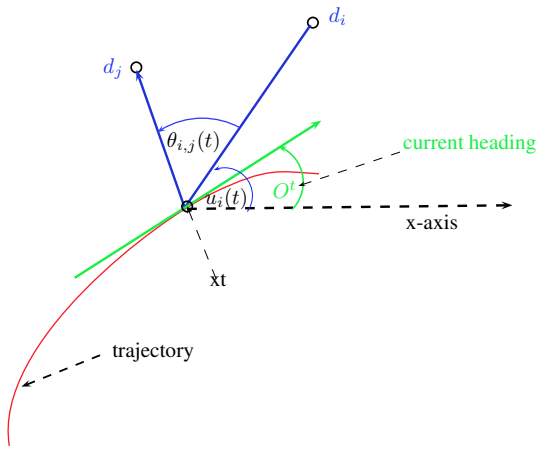

Fig. 2. figure shows the heading angle O^t, $\mu_{ij}(t)$ and $\mu_i(t)$ at time t

B. Notations

As described in BHMIP Let $D = \{\mathbf{d^1}, \mathbf{d^2}, ..., \mathbf{d^m}\}$ be the set of final destinations a person can go to in a given environment. These destinations represent the inherent intentionality of a person. We use the expectation maximization to compute them for a given environment [14]. Human trajectories are represented as $X(T) = \{\mathbf{x^1}, \mathbf{x^2}, ..., \mathbf{x^T}\}$ where $\mathbf{x^t} = (x^t, y^t)$ is position of the person at time t with respect to the global reference frame and the superscript T indicates the total number of points in the trajectory. As shown in the Fig. 2, O^t is the angle defined by the first derivative of the trajectory at point $\mathbf{x^t}$. Given the current position and orientation we compute the probability of reaching each of the destination $d^i \in D$. Indeed these probabilities represent the intent/intentional probability of the human in consideration to pursue those destinations. We pose the problem of finding these probabilities as an HMM problem.

C. Proposed Approach

Let $S^t \in D$ represent the intent of a person to reach destination S^t at time t. As mentioned earlier D is the set of final locations a person can reach in the given environment and it also represents the set of states in the HMM. O^t as shown in Fig. 2 , is the heading of the person at time t and it is calculated using the trajectory information $X(T)$ provided by the sensor. The heading measurement probability $b_i(O^t)$ is defined as the probability of observing heading O^t given that the person is following the intent $\mathbf{d^i}$ at time t. According to BHMIP this can be given as

$$b_i(O^t) = p(O^t|S^t = \mathbf{d^i}) = \mathcal{N}(O^t|\mu_i(t), \sigma_o)$$

As shown in the Fig. 2, $\mu_i(t)$ is the slope of the line joining the points $\mathbf{x^t}$ and $\mathbf{d^i}$. In BHMIP paper it has been argued that there exist a high similarity between the O^t pdf and a Gaussian function which has been modeled using the above normal distribution. $\mu_i(t)$ is the measure relative to the destination $\mathbf{d^i}$ and O^t is the global measure of the target orientation. If the heading angle is close to $\mu_i(t)$ we get a high value of $b_i(O^t)$ and vice versa . We represent the transition probability i.e the probability that the human changes his intent from $\mathbf{d^i}$ to $\mathbf{d^j}$ at any discrete instant t as $a_{ij}(t)$ and use the same concept used in BHMIP to define it as follows:

$$a_{ij}(t) = p(S^{t+1} = \mathbf{d^j}|S^t = \mathbf{d^i}) = \eta\mathcal{N}(\theta_{ij}(t)|0, \sigma_a)$$

As shown in the Fig. 2, $\theta_{ij}(t)$ is the angle between the lines joining the points $\mathbf{x^t}$ to $\mathbf{d^i}$ and $\mathbf{x^t}$ to $\mathbf{d^j}$ and it represents the measure between final destinations $\mathbf{d^i}$ and $\mathbf{d^j}$ relative to the current position $\mathbf{x^t}$.The smaller this angle the larger the value of transition probability $a_{ij}(t)$ which suggest the high chances of transition in intent from $\mathbf{d^i}$ to $\mathbf{d^j}$ at time t. η is the normalization constant which can be given as

$$\eta = \sum_{j=1}^{m} a_{ij}(t)$$

Our task is to calculate $p(S^t = \mathbf{d^i}|O^{1:T}, \lambda)$ i.e the probability that a person follows the intent $\mathbf{d^i}$ at time t, in the above term λ is the set of HMM parameters and $O^{1:T} = \{O^1, O^1, ..., O^T\}$ is the set of measurements obtained till time T. In HMM this term is usually referred to as $\gamma_t(i)$ and To find this we use forward and backward algorithms. In HMM The forward parameter $\alpha_t(i)$ is defined as

$$\alpha_t(i) = p(S^t = \mathbf{d^i}, O^{1:t}|\lambda)$$

which can be further simplified as

$$\alpha_t(i) = \left[\sum_{i=1}^{m} \alpha_{t-1}(j)a_{ji}\right] b_i(O^t)$$

The backward parameter $\beta_t(i)$ is defined as

$$\beta_t(i) = p(O^{t+1:T}|S^t = \mathbf{d^i}, \lambda)$$

Which can be further simplified as

$$\beta_t(i) = \sum_{i=1}^{m} a_{ij}(t)b_j(O^{t+1})\beta_{t+1}(j)$$

The term $p(S^t = \mathbf{d^i}|O^{1:T}, \lambda)$ can be further simplified in terms of forward and backward parameters.

$$p(S^t = \mathbf{d^i}|O^{1:T}, \lambda) = \frac{p(S^t = \mathbf{d^i}, O^{1:T}, \lambda)}{p(O^{1:T}, \lambda)}$$
$$= \frac{p(S^t = \mathbf{d^i}, O^{1:T}|\lambda)}{p(O^{1:T}|\lambda)}$$
$$= \frac{p(S^t = \mathbf{d^i}, O^{1:t}, O^{t+1:T}|\lambda)}{p(O^{1:T}|\lambda)}$$
$$= \frac{p(O^{t+1:T}|S^t = \mathbf{d^i}, O^{1:t}, \lambda)p(S^t = \mathbf{d^i}, O^{1:t}|\lambda)}{p(O^{1:T}|\lambda)}$$
$$= \frac{\alpha_t(i)\beta_t(i)}{\zeta}$$

where ζ can be given as

$$\zeta = \sum_{i=1}^{m} \alpha_t(i)\beta_t(i)$$

$$\Rightarrow \gamma_t(i) = \frac{\alpha_t(i)\beta_t(i)}{\sum_{i=1}^{m} \alpha_t(i)\beta_t(i)}$$

As mentioned $\gamma_t(i)$, is the probability that the person follows intent $\mathbf{d^i}$, at time t.

IV. Modeling uncertainties along each intent

On assumption of linear system dynamics, we have the following equations,

$$x^t = Ax^{t-1} + B^t u^t + \varepsilon^t \tag{1}$$

Where,x^t is the state of a particular intent trajectory at time t, and u^t is the control variable that is taken as velocity. ε^t is a random variable with zero mean and covariance given by R^t. If nonlinear system dynamics is considered which is of the form,

$$x^t = g(u^t, x^{t-1}) + \varepsilon^t \tag{2}$$

Then 2 is linearized appropriately to get an equation which is similar to 1.Now under linear system dynamics,the p.d.f of x^t given in 1, is a Gaussian distribution with parameters given by,

$$\mu^t = A^t\mu^{t-1} + B^t\mu^t \tag{3}$$

$$\Sigma^t = A^t(\Sigma^{t-1}A^t)^T + R^t \tag{4}$$

The μ^t and Σ^t is given by 3 and 4, are considered in the later sections of this paper, while formulating the probabilistic variant of the *time scaled collision cone* constraints.

V. Collision Avoidance with Time Scaled Collision Cone and Its Probabilistic Variant

In this section, we provide a brief review of the concepts developed in our earlier works [3], [4]. These cited works explain how it is advantageous to first project and solve collision avoidance along a particular path and then subsequently evaluate the obtained closed form solution along multiple candidate paths. Thus, in this section, we first explain the concept of time scaling which is used to obtain the path constrained version of collision cone constraints [7]. The resulting constraints are labeled as *time scaled collision cone* constraints.Thereafter, we develop a probabilistic version of the time scaled cone. For the lack of space, the theoretical exposition is significantly shortened; the readers are requested to refer to supplementary material [16] for a detailed explanation.

A. Time Scaled Collision Cone Constraints

The *time scaled* or path constrained version of the collision cone constraints can be obtained by changing the current time scale, t to the new time scale, τ in the trajectory definition $\mathbf{X}^t$. Such transformations do not alter the geometric path of the current trajectory but brings the following change in the velocity and acceleration profile.

$$\dot{\mathbf{X}}^\tau = \dot{\mathbf{X}}^t \frac{dt}{d\tau}, \ddot{\mathbf{X}}^\tau = \ddot{\mathbf{X}}^t (\frac{dt}{d\tau})^2 + \dot{\mathbf{X}}^t \frac{d^2t}{d\tau^2} \tag{5}$$

It is easy to understand from (5) that *time scaling* transformation results in change of velocities and accelerations through change in the temporal profile of the trajectory. In (5) $\frac{dt}{d\tau}$ is called the scaling function and decides the transformation between the time scales. By denoting $\frac{dt}{d\tau}(t_c) = s$ the set of velocities that the robot can attain at time t_c through scaling transformation can be denoted as $(s\dot{x}^{t_c}, s\dot{y}^{t_c})$. Thus, the *time scaled* version of collision cone constraints take the following form. Readers are requested to refer to [3], [4], [16] for some more details leading to the following set of constraints.

$$f_i^s \geq 0, \forall i = 1, 2...n \tag{6}$$

$$f_i^s = (x^{t_c} - x_i^{t_c})^2 + (y^{t_c} - y_i^{t_c})^2 - R^2 - \frac{(s\dot{x}^{t_c} - \dot{x}_i^{t_c})(x^{t_c} - x_i^{t_c}) + (s\dot{y}^{t_c} - \dot{y}_i^{t_c})(y^{t_c} - y_i^{t_c})^2}{(s\dot{x}^{t_c} - \dot{x}_i^{t_c})^2 + (s\dot{y}^{t_c} - \dot{y}_i^{t_c})^2}, \forall i = 1, 2...n \tag{7}$$

As can be deduced from (6), *time scaled* collision cone constraints represents single variable quadratic inequalities in the form $a_i s^2 + b_i s + c_i \geq 0$. The symbolic formulae depicting the solution space of s are presented in [4].

B. Probabilistic Variant of Time Scaled Collision Cone Constraints

Now, consider the case where the obstacle trajectories are represented as probability distributions. Without loss of generality and for the sake of simplicity of theoretical exposition let us assume that the obstacle states at any time t can be represented as below in the form of Normal Distributions, obtained through the methodology presented in section IV. The following theory is valid for other parametric distributions as well.

$$x_i^{t_c} \sim N(\mu_i^x, \sigma_i^x), \dot{x}_i^{t_c} \sim N(\mu_i^{\dot{x}}, \sigma_i^{\dot{x}}) \\ y_i^{t_c} \sim N(\mu_i^y, \sigma_i^y), \dot{y}_i^{t_c} \sim N(\mu_i^{\dot{y}}, \sigma_i^{\dot{y}}) \tag{8}$$

In (8), μ_i^x, σ_i^x, $\mu_i^{\dot{x}}$, $\sigma_i^{\dot{x}}$ and similar others are mean and standard deviation associated with respective component of the predicted states of the i^{th} obstacle. With respect to (8), f_i^s now becomes a multivariate function of random variables and thus consequently a random variable itself. Thus, (6) can be interpreted a set of constraints on the possible outcome of the random variables f_i^s. In other words, (6) can be replaced with the following chance constraints. In (9), ϵ is some positive number and we want to ensure (9) for as large as possible value of ϵ.

$$Pr(f_i^s \geq 0) \geq \epsilon \tag{9}$$

Now, consider the following family of deterministic algebraic constraints where $\mu_{f_i^s}$ and $\sigma_{f_i^s}$ are respectively the mean and standard deviation of $\sigma_{f_i^s}$. As shown in [16], these terms can be derived in symbolic form as a function of the variable s.

$$\mu_{f_i^s} \pm k_i \sigma_{f_i^s} \geq 0 \tag{10}$$

Now, satisfaction of (10) leads to the following probability bounds derived through Cantelli's inequality.

$$Pr(f_i^s > \mu_{f_i^s} + k_i\sigma_{f_i^s}) \leq \frac{1}{1+k_i^2}, Pr(f_i^s > \mu_{f_i^s} - k_i\sigma_{f_i^s}) \geq \frac{k_i^2}{1+k_i^2} \tag{11}$$

Thus, satisfaction of (10) would ensure the satisfaction of the chance constraints (9) with $\epsilon = \frac{k_i^2}{1+k_i^2}$. Consequently, we can replace the chance constraints with a family of deterministic constraints. Equivalently, our objective would now be to satisfy (10) for as large as possible value of k_i.

Now, we have shown in [16], that (10) can be effectively approximated through quadratic inequalities in terms of single variable s and thus, can be solved in closed form, along with an adequate justification on the lower bounds of (9) and its dependency on the variable k_i.In the next section, we adapt the formulations discussed till now for developing a proactive navigation in human centered environments.

VI. Collision Avoidance in the Intent Space

As mentioned earlier, the intent space is characterized by human intents characterized by probabilities and the uncertain trajectories leading to those intents. For example, consider figure 3, where the trajectories shown in red, blue and green characterize the intent space. The uncertainty associated with each intent trajectory at time t_c (the collision instant) are shown as grey ellipse.

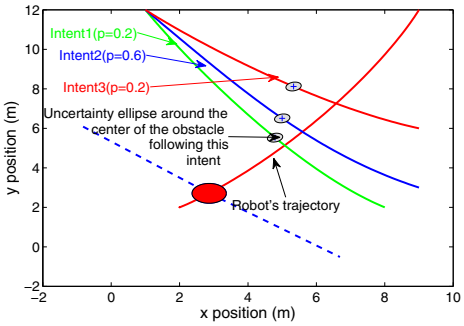

Fig. 3. Figure shows the robot's current trajectory, along with various intents (taken by the person), with associated probabilities and uncertainty ellipses

In this section, we transport the formulation of avoiding uncertain trajectories discussed in the previous section to intent space. Specifically we extract a specific solution from the entire solution space depending on factors like deviation from the current path, acceleration/de-acceleration capability of the robot and confidence of collision avoidance. Keeping up with the discussions of the previous section, we first propose an optimization framework which extracts a particular solution for avoiding collisions along the current geometric path. We can then subsequently repeat the optimization over multiple homotopic paths to further improve the solution.

We start with the following optimization problem

$$\min J_{cost} = w_t\Delta_t + w_p\Delta_r \\ \mu_{f_i^s} \pm k_i\sigma_{f_i^s} \geq 0 \tag{12}$$

$$\Delta_t = (s-1)^2 \tag{13}$$

$$\Delta_r = -\sum_i^n \gamma_i k_i \tag{14}$$

In (12), the total cost J_{cost} is comprised of two individual costs Δ_t and Δ_r which respectively penalizes deviation current temporal profile and the risk associated with the avoidance maneuver. w_t and w_p are the weights characterizing the relative importance of each term. It can be easily noted that Δ_t is modeled based on the fact that $\frac{dt}{d\tau}(t_c) = s \approx 1$ would result in a velocity profile very close to the current values and thus would require minimal acceleration/de-acceleration change. In other words, Δ_t ensures a collision free velocity very close to the current velocity value which in turn would be easy for the robot to reach. The term Δ_r is modeled based on the fact that the confidence measure increases in direct relation with k_i and thus maximizing it or equivalently minimizing its negative would improve the confidence and consequently reduce risk. The individual k_is are weighted by the probability γ_i of the corresponding intent. This biases the

solution towards avoiding the most likely intent with higher confidence.

The structure of the optimization is fairly simple. The objective function is combination of a linear term in terms of variable k_i and a convex quadratic in terms of variable s. The constraints can be well approximated through quadratic inequalities in terms of variable s and k_i (refer [16]) by linearizing $\sigma_{f_i^s}$ with respect to s. Now, depending on the obstacle configuration, these quadratic inequalities can be convex or non-convex. In case of non-convex quadratic inequalities, we reformulate them into the so called *difference of convex form* [5]. Thus, even in the case of non-convex instance, the optimization (12) can be efficiently solved through state of the art methods like *sequential convex programming*[5]

As an example, we solve the optimization (12) with $w_t = w_p = 1$ for the collision scenario shown in figure 3, which comprises of three intent trajectories. The solution of the optimization returns $s = 0.6$. The confidence associated with the collision free velocity characterized by this particular value of s is given by the k_is which in this case are obtained as $k_1 = 0.92, k_2 = 1.64, k_3 = 2.0$. We present figures 4(a)-4(d) to graphically validate the obtained solutions. For example, figure 4(a) shows the cost function along with the limiting constraints. To understand what we mean by limiting constraints, note from (12) that each intent trajectory induces a pair of constraints and thus, the solution space is dictated by the constraint which has minimum (limiting) value. For clarity, we also plot the constraints separately in figures 4(b)-4(d), where we show both the limiting and non-limiting component of each constraint.

Coming back to figure 4(a), it can be easily noted that the limiting constraints are satisfied (greater than zero) to the left of $s = 0.6$, suggesting that it is indeed the value closest closest to one (refer (13)) for the obtained values of k_i.

A. Evaluating Optimization (12) over multiple Candidate Paths/Trajectories.

In the last section, we learned how to compute an optimal and safe collision free velocity that the robot can attain by just changing the temporal profile of the trajectory while not deviating from the current path. However, sometimes it may become imperative to deviate from the current path, to avoid collisions. For example, consider the collision scenario shown in figure 5, which is obtained by slightly altering the configuration of the intent trajectories from figure 3. As summarized in table I, no solution is obtained along the current path, suggesting the need to repeat the optimization (12) along other candidate paths/ trajectories.

As an example, consider figure 5, where we generated three candidate trajectories following the approach of [4]. The output of the optimization (12) along each of these candidate paths/ trajectories is graphically demonstrated in figures 6(a)- 6(c), while table I provides a quantitative summary of the results. It can be seen that the deviation from the current path increases from candidate trajectory 1 to candidate trajectory 3. As shown in table I, this gradual

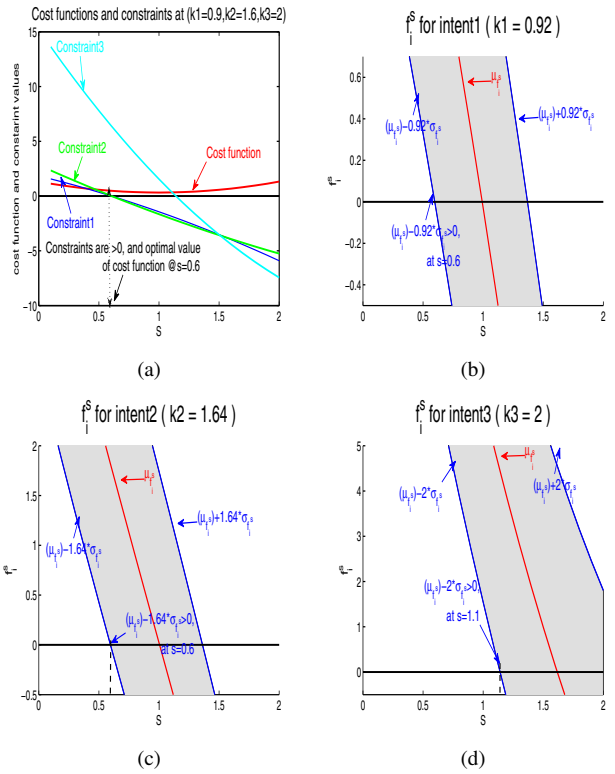

Fig. 4. Figure (a) shows the plot of the cost function in 12 and limiting constraints, while (b)-(d) show the plots of both the limiting and non limiting constraints, for the collision scenario shown in figure 3. The area that is shade in grey in figures (b)-(d) directly corresponds to the confidence meausure of avoiding each intent.

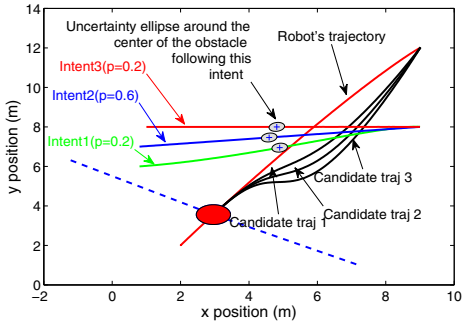

Fig. 5. Plot of possible candidate trajectories for the robot. The cost function 15 decides which of these trajectories is chosen by the robot.

increase in deviation correspondingly maps to the improvement in the solution of collision free velocity (variable s) and its associated confidence bounds.

Now, to resolve this redundancy in solutions and pick a particular candidate trajectory, we modify the cost function in (12) in the following manner

$$J_{cost} = w_p\Delta_p + w_t\Delta_t + w_r\Delta_r \tag{15}$$

In (15), Δ_p measures the deviation from the current path [4]. It is clear that the choice of a particular candidate trajectory would be dictated by the relative magnitude of w_p as compared to w_t and w_r. For example, for the collision

scenario of 5, if w_p is set much higher than w_t and w_r, then candidate trajectory 1 is chosen. Similarly, $w_p \approx w_t \approx w_r$ results in the choice of candidate trajectory 2.

In the next section, we apply the theoretical exposition presented till now and showcase some additional simulation results as well as real time navigation of a non-holonomic mobile robots among human obstacles.

TABLE I

SCALE AND CONFIDENCE TABLE FOR THE ROBOT'S PERTURBED TRAJECTORIES

Candidate trajectories	k1	k2	k3	scale(s)
Robo original traj	Null	Null	Null	Null
Candidate traj.1	0.2	2	2	0.6
Candidate traj.2	0.67	2	2	0.916
Candidate traj.3	1.72	2	2	1

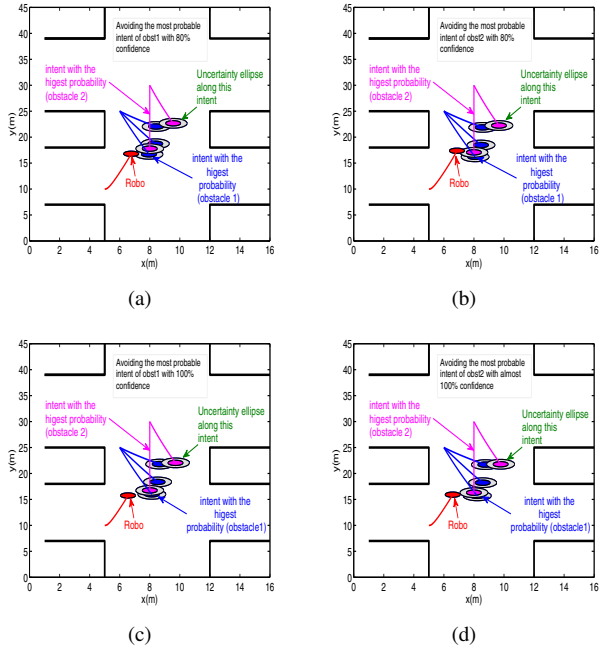

Fig. 7. A typical collision scenario in corridor like spaces with two obstacles (humans). The intents along with their probabilities are shown in the figure. Figures 7(a),7(b),clearly show that,the robot is avoiding the most probable intents of obstacle 1 and 2 with 80% confidence, and figures 7(c),7(d), show that the most probable intents of obstacle 1 and 2 are avoided with almost 100% confidence.

VII. ADDITIONAL RESULTS AND DISCUSSIONS

In this section, we present some additional simulation results as well as experimental results. Due to the lack of space, only some results are shown. The readers are requested to refer to the video [18] for the better understanding of the results.

A. Collision Avoidance in Corridors

Figures 7(a)-7(d) show snapshots of collision avoidance with two human obstacles in tight spaces like corridors. Figures 7(a)- 7(b) summarizes the avoidance maneuver corresponding to 80% confidence, while 7(c)- 7(d) depicts the avoidance with almost 100% confidence.Situations similar to that of head-on collisions in constrained spaces has been simulated in our past work [4], where the robot adopts reversals to ensure collision avoidance.

B. Real Time Implementation

For the physical implementation we used Microsoft Kinect [17] to detect the location of humans in the indoor environment and performed collision avoidance on a Pioneer 3DX differential drive robot. We performed several experiments to validate our approach. Only one result is shown here; the video [18] summarizes other results.

The position of pedestrians are detected using the skeleton grab API of a Kinect camera.Figures (8(a),8(b),8(c)) represents a typical run with the positions of the robot and the person displayed. Figures (8(d),8(e),8(f)), shows the corresponding plots generated in rviz, giving details about the possible final destinations(pink cubes), probability of various intentions(various arrows) and robot's trajectories(blue and green). The trajectory shown in green in these figures is the robot's current geometric path, and the trajectory in blue is the robot's best candidate trajectory resulting from the optimization structure mentioned in section VI.

VIII. CONCLUSIONS AND FUTURE WORK

We presented an efficient collision avoidance framework for non-holonomic robots operating in human centered environments. The framework explicitly considers the probability of each intent of the human and the uncertainty associated with the trajectory leading to each intent. The proposed framework, which is based on the probabilistic variant of previously developed *time scaled collision cone* concept, is quite unique as compared to the existing works, in the sense that it does not require explicit sampling in the state and control space of the robot. Building on the closed form characterization of collision free velocities and the associated confidence bounds, we proposed an optimization framework to obtain an avoidance maneuver which elegantly balances the ease and risk of collision avoidance. The optimization framework was shown to have either a convex or *difference of convex* form, and thus can be solved efficiently.

At the moment, we are extending the current formulation to include robot's uncertainty.

REFERENCES

[1] M. Bennewitz,W. Burgard, G. Cielniak, S. Thrun: Learning motion patterns of people for compliant robot motion. Int. J. Robot. Res. 24(1), 31-48 (2005)

[2] D. Vasquez, T. Fraichard, and C. Laugier,Growing hidden markov models: An incremental tool for learning and predicting human and vehicle motion,The International Journal of Robotics Research, vol. 28, no. 11-12, pp. 1486-1506, 2009

[3] Singh, A. K., and Krishna, K. M. (2013, December). Reactive collision avoidance for multiple robots by non linear time scaling. In Proc. of IEEE CDC 2013 (pp. 952-958).

[4] Gopalakrishnan, B., Singh, A. K., and Krishna, K. M. (2014, September). Time scaled collision cone based trajectory optimization approach for reactive planning in dynamic environments. In Proc. of IEEE IROS 2014 (pp. 4169-4176).

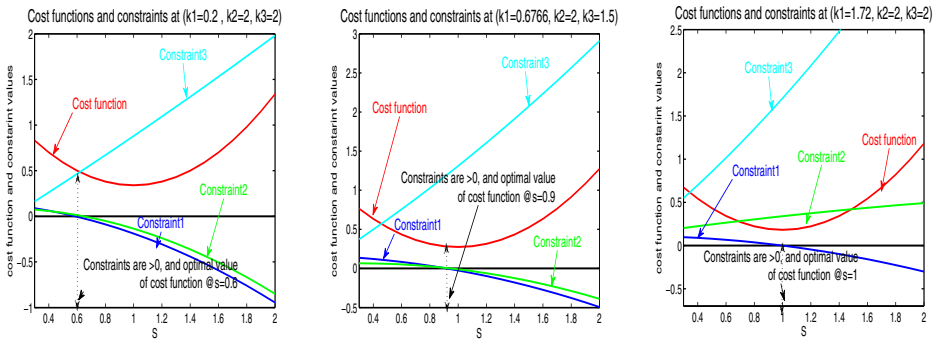

(a) (b) (c)

Fig. 6. (a)-(c): Plots of constraints and cost function for robot's candidate trajectory 1, 2, 3 respectively. The plots are qualitatively similar to that presented in figures 4(a). It can be seen that the constraints are satisfied to the left of the optimal s, suggesting that it is indeed the value closest to one, thus conforming to the objective 13

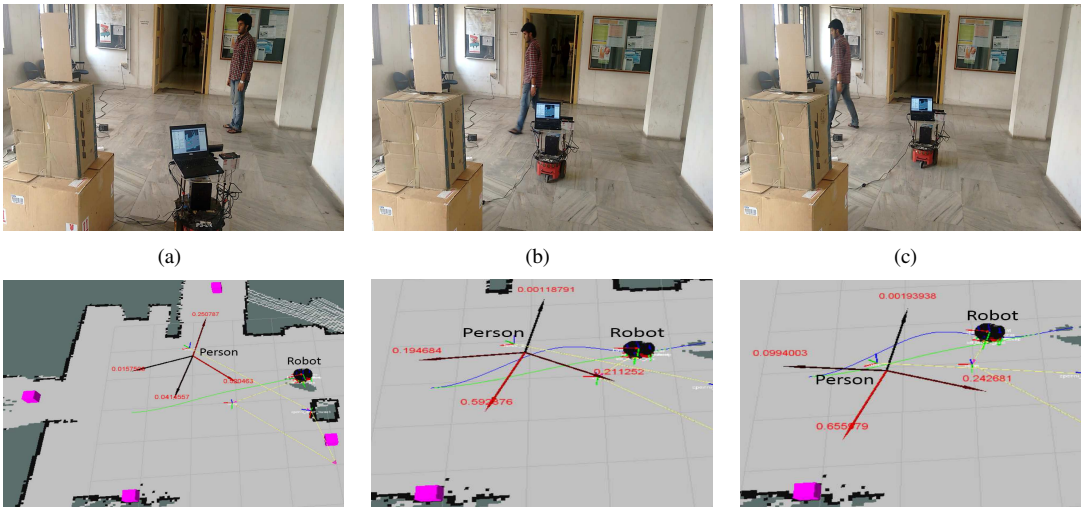

(a) (b) (c)

(d) (e) (f)

Fig. 8. (a),(b) and (c) shows the robot changing its trajectory to avoid a person and (d),(e) and (f) shows corresponding trajectories and robot's motion on rviz.

[5] Boyd, S. (2008). Sequential convex programming. Lecture Notes, Stanford University.

[6] Fiorini, P., and Shiller, Z. (1998). Motion planning in dynamic environments using velocity obstacles. IJRR, 17(7), 760-772.

[7] Chakravarthy, A., and Ghose, D. (1998). Obstacle avoidance in a dynamic environment: A collision cone approach. Systems, Man and Cybernetics, Part A: Systems and Humans, IEEE Transactions on, 28(5), 562-574.

[8] van den Berg, J., Snape, J., Guy, S. J., and Manocha, D. (2011, May). Reciprocal collision avoidance with acceleration-velocity obstacles. In Robotics and Automation (ICRA), 2011 IEEE International Conference on (pp. 3475-3482). IEEE.

[9] Alonso-Mora, J., Breitenmoser, A., Beardsley, P., and Siegwart, R. (2012, May). Reciprocal collision avoidance for multiple car-like robots. In Robotics and Automation (ICRA), 2012 IEEE International Conference on (pp. 360-366). IEEE.

[10] Kushleyev, A., and Likhachev, M. Time-bounded lattice for efficient planning in dynamic environments. In Proc. of IEEE ICRA 2009 (pp. 1662-1668).

[11] Fulgenzi, C., Tay, C., Spalanzani, A., and Laugier, C. (2008, September). Probabilistic navigation in dynamic environment using rapidly-exploring random trees and gaussian processes. In Proc. IEEE IROS 2008 (pp. 1056-1062).

[12] Ferrer, G., and Sanfeliu, A. (2014, September). Proactive kinodynamic planning using the Extended Social Force Model and human motion prediction in urban environments. In Intelligent Robots and Systems (IROS 2014), 2014 IEEE/RSJ International Conference on (pp. 1730-1735). IEEE.

[13] Singh, A. K., Krishna, K. M., and Saripalli, S. (2012, October). Planning trajectories on uneven terrain using optimization and non-linear time scaling techniques. In Intelligent Robots and Systems (IROS), 2012 IEEE/RSJ International Conference on (pp. 3538-3545).

[14] Ferrer, G., and Sanfeliu, A. (2014). Bayesian human motion intentionality prediction in urban environments. Pattern Recognition Letters, 44, 134-140.

[15] L. Rabiner, A tutorial on hidden markov models and selected applications in speech recognition. In: Readings in Speech Recognition, pp. 267-296 (1990)

[16] Efficient Computation of the Space of Safe Velocities for Non-Holonomic Robots in Uncertain Dynamic Environments, Arun Kumar Singh,K. Madhava Krishna, February 2015. Report no: IIIT/TR/2015/3.(pdf)

[17] Microsoft Corp. Redmond WA. Kinect for Xbox 360

[18] https://www.youtube.com/watch?v=FatDe-BwB6M&feature=youtu.be